UNITED NATIONS UNIVERSITY

GEOTHERMAL TRAINING PROGRAMME
Orkustofnun, Grensasvegur 9,
IS-108 Reykjavik, Iceland

Reports 2010
Number 30

RESOURCE ASSESSMENT OF TOMPASO GEOTHERMAL FIELD, INDONESIA

Bayu Tri Handoko
Pertamina Geothermal Energy
Menara Cakrawala 15th Floor
Jl. MH. Thamrin 9, Jakarta
INDONESIA
bayutrihandoko@pertamina.com

ABSTRACT

The Tompaso geothermal field is one of the prospect fields being developed by PT. Pertamina Geothermal Energy. The Tompaso prospect is located in North Sulawesi, Indonesia about 30 km from the Lahendong geothermal field which currently produces about 60 MW_e. In 2008, the first exploration well was drilled in Tompaso and today there are a total of 8 wells divided into 3 clusters. The purpose of the drilling activity is to develop a 2×20 MW_e power plant, i.e. units 5 and 6 in Tompaso Prospect. This paper describes a resource assessment of the Tompaso geothermal field that consists of volumetric calculations for 20, 25 and 30 year production scenarios. A well test analysis for the purpose of calculating transmissivity and storativity values is also described. The well testing utilised all existing data from step drawdown tests in the Tompaso geothermal field. The last chapter describes pressure drawdown calculations using the Monte Carlo method to simulate pressure decline in the Tompaso prospect for different production scenarios in order to optimise future production.

1. INTRODUCTION

The Tompaso geothermal prospect is located in the administrative district of Minahasa, North Sulawesi Province in Indonesia, located roughly 60 km south of Manado city, the capital city of the North Sulawesi Province (Figure 1). Geographically, the Tompaso geothermal prospect is bounded by 01 09’ 02’ and 01 11’ 32’ North Latitude and 124 47’ 19’and 124 49’ 49’ East Longitude, or 126 – 136 N and 696 – 706 E.

The Tompaso geothermal field is one of the geothermal fields included within the Lahendong concession. With increased demand for electricity in North Sulawesi which cannot be handled by the Electric National Company, further development of geothermal energy in North Sulawesi is necessary in order to fulfil the demand. After further surface exploration, the next step is to begin exploration drilling to obtain a higher certainty regarding the dimensions of the reservoir and the amount of proven reserves in Tompaso geothermal prospect.

Currently in Tompaso there are plans to develop power plant units 5 and 6 in order to increase the electrical supply in North Sulawesi. Since September 2008, 8 wells have been drilled in the Tompaso

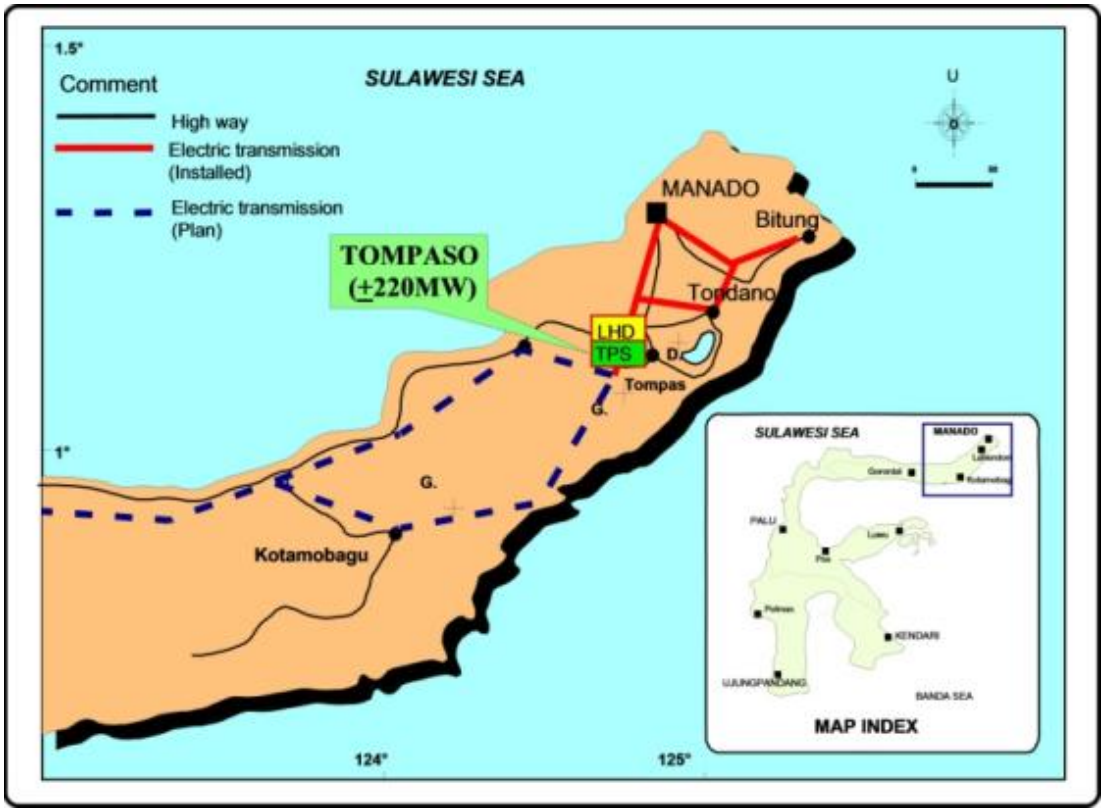

FIGURE 1: Location of the Tompaso prospect (PGE, 2008)

geothermal field, grouped into 3 different clusters. These 8 wells consist of 2 exploration wells LHD-26 and LHD-27), 4 production wells (LHD-30, LHD-31, LHD-33 and LHD-34) and 2 injection wells (LHD-32 and LHD-35). A conceptual model of the Tompaso geothermal field was made using data from drilling and well tests. In addition, there exist production test data from wells LHD-27 and LHD-34, used as supporting data in building the conceptual model.

2. TOMPASO GEOTHERMAL FIELD BACKGROUND

2.1 Geology

Tompaso prospect area is located on the north arm of Sulawesi Island which is part of a series of SW-NE trending volcanoes, including Mount Klabat, Mount Mahawu, Mount Soputan and Mount Ambang. Tompaso prospect contains the large caldera lake Tondano which was produced in Plio-Pleistocene times. The prospect is also part of the massive complex of the Lembeyan volcanic cluster which is bounded on the north by the active Mahawu and Lokon volcanoes, and on the south by Mount Soputan, Mount Sempu and Mount Rindangaen. The Lake Tondano lies to the east.

The volcanic rocks in the area consist of pyroclastic tuff overlying pumice, both of which are covered by Quaternary volcanic products (Figure 2). Tompaso geothermal prospect is located in a relatively flat depression with an average elevation of 750 m a.s.l. The active volcano Mount Soputan is suspected to affect the deep hydrology of Tompaso prospect, and lies to the west. Mount Sempu is located northeast of Mount Soputan and shows traces of a caldera that is no longer active.

Shallow borehole core data shows that the Tompaso prospect was initially covered by a lake or some kind of surface water. As a result of tectonic activity, the Lahendong region partly lifted and tilted

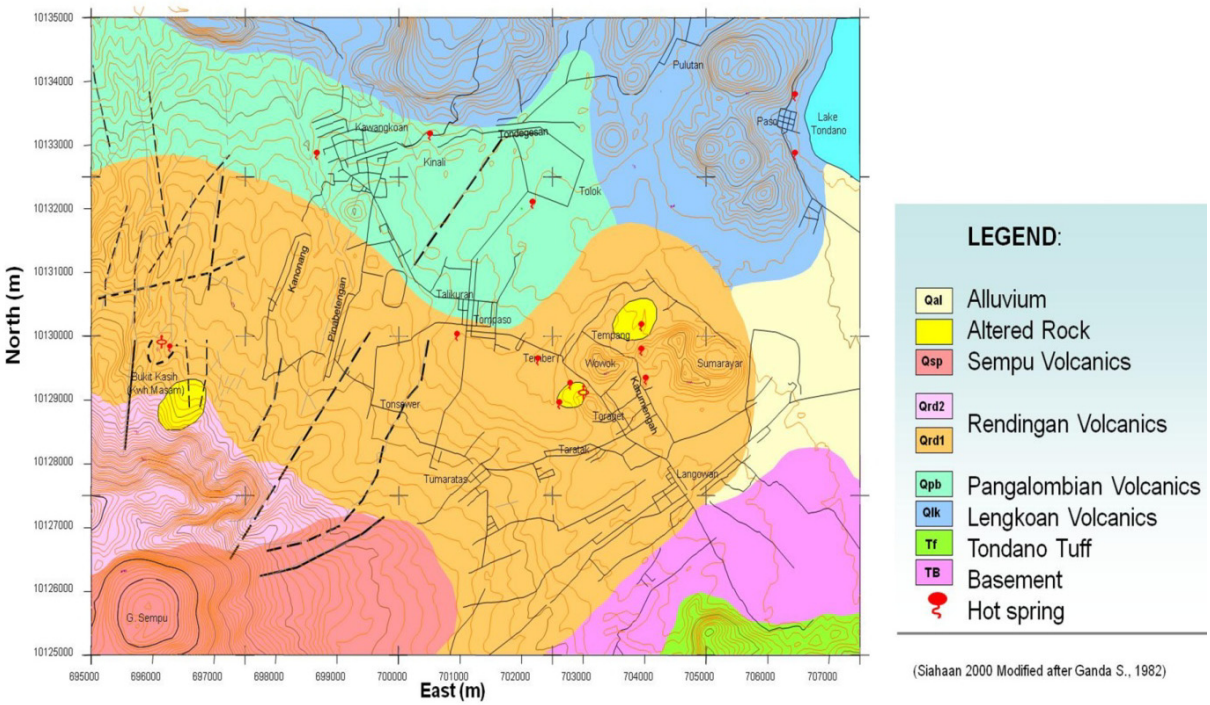

FIGURE 2: Geological map of Tompaso (PGE, 2008)

causing new eruptions from Mount Rindangen, Mount Soputan, Mount Lengkoan, Mount Tampusu and Mount Kasuratan.

Fault structures were interpreted from aerial photographs. Several structures were derived:

- Regional lineaments with NE-SW and NW-SE trends;
- NE-SW fault through Mount Damaah, Mount Masarang, complex volcanic Tampusu-Kasuratan and complex Sempu-Soputan;
- Normal fault facing southwest of Mount Lengkoan Peak;
- Fault trending NW-SE through the river Bapaluan, the Tempang manifestations area and the mountains of southeast Lembeyan; and
- E-W fault through two regional alterations – Batukolok, in Mount Rindengan and Tompaso and Tempang.

These faults have a major influence on the hydrologic system in the area and are major surface features in the Tompaso geothermal manifestation.

Based on geological evidence, it appears that the magmatic evolution expected as a heat source moved from the northeast to the southwest, from Mount Lengkoan to Mount Sempu, Mount Rindengan-Maniporok-Aesoput and finally Mount Soputan. Therefore, the heat sources that currently exist are relatively shallow and are derived from Mount Soputan. The regional faults produce a high permeability zone trending NE-SW through the area.

2.2 Geochemistry

The geochemistry of the Tompaso area is divided into three main water element types: chloride, bicarbonate and sulphate.

Chloride water type
Chloride hot springs are common in the central part of the prospect in Tempang (Karumengah) area. The chloride hot springs occur when geothermal water mixes with shallow groundwater and sedimentary rocks with high boron content. The hot springs range are found at an elevation of approximately 710 m a.s.l. and they are pH neutral; the temperatures range from 73 to 97°C.

Sulphate water type
Sulphate hot springs are located in the Tempang area, Mount Soputan, Masam crater and Totolan and are identified by steamy water, steaming ground, and mud pools with low water discharge. These manifestations are formed above the water table where the steam heats the water surface, causing H_2S gas to react with oxygen, becoming H_2SO_4, and changing the pH from neutral to acidic. These sulphate hot springs occur at elevations ranging from 710 to 910 m a.s.l. and range in temperature from 77 to 86°C.

Bicarbonate water type
The bicarbonate water type covers the majority of the study area, especially in the plains at low elevations between 450 and 710 m a.s.l. (Remboken, Kinali, Pinabetengan, Ranowangko). Bicarbonate water is produced by surface water runoff mixing with water from the reservoir that comes into shallow surface water features (lakes) such as Tondano lake in Remboken area. This water has a high magnesium concentration.

Geographically, the geothermal manifestations in the Tompaso area are divided into four different regions:

- Manifestations in Tempang - Tompaso - Mount Umeh area which is dominated by chloride hot springs, mud pools, acidic hot springs and steaming ground;
- Manifestations in Masam crater – Mount Rindengan area which is dominated by fumaroles, solfatara and hot springs;
- Manifestations in Kawangkoan – Mount Emung area which is dominated by bicarbonate and sulphate hot springs; and
- Manifestations that appear on the edge of Tondano lake and Remboken village and are dominated by bicarbonate hot springs.

2.3 Geophysics

Schlumberger resistivity
Resistivity maps (Schlumberger with AB/2 = 500 m and AB/2 = 1000 m) show two main prospects in the Tompaso area. At shallow depths, a tongue shaped structural pattern indicates the existence of fluid flow that moves from west to east in Masam crater towards Tompaso and Tempang.

Magneto-telluric resistivity
From the MT resistivity data with T = 3 s and T = 1 s (skin depth) at 2000 m depth, two prospects with a resistivity value of 5-10 ohm-m can be seen (Figures 3 and 4). The main prospect is located in Masam Crater (Mount Rindengan) and the second prospect is located in Tompaso and Tempang. A conductive layer with a thickness ranging from 750 to 1000 m occurs at the Masam crater reservoir, and the top of the reservoir is around sea level (Figure 3). The top of the reservoir in Tempang-Tompaso is around 500 m below sea level depth (b.s.l.). The MT data reveals a conductive layer in both prospects with a value between 3 -5 ohm-m which indicates argillic altered rocks about 750-1000 m thick.

From the MT cross-section (Figure 3), it can be seen that the two prospects are separated by a barrier structure which is large and not manifested at the surface. It is not possible that, at depth, both prospects come from the same reservoir.

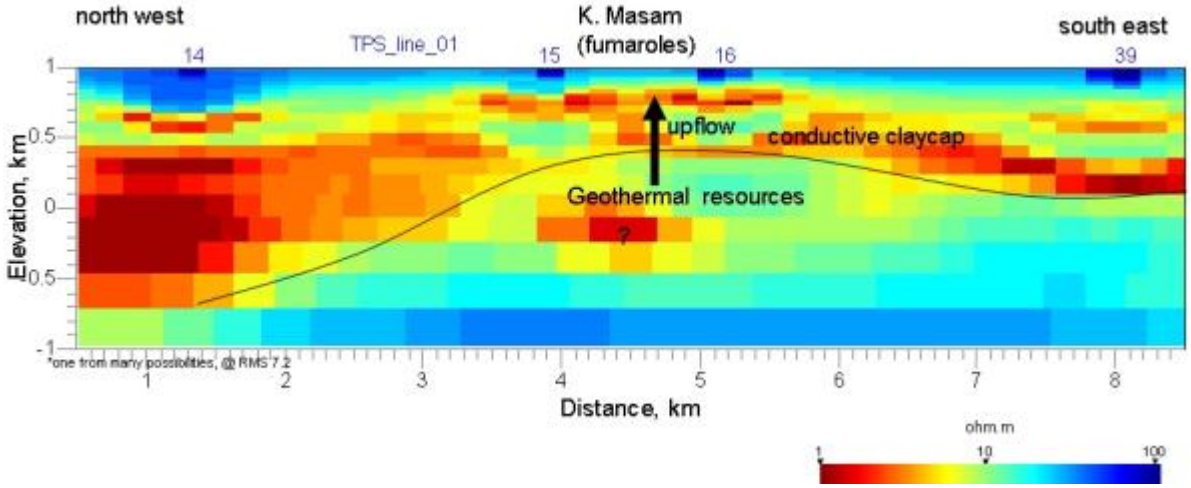

FIGURE 3: MT cross-section of the Tompaso prospects (PGE, 2008)

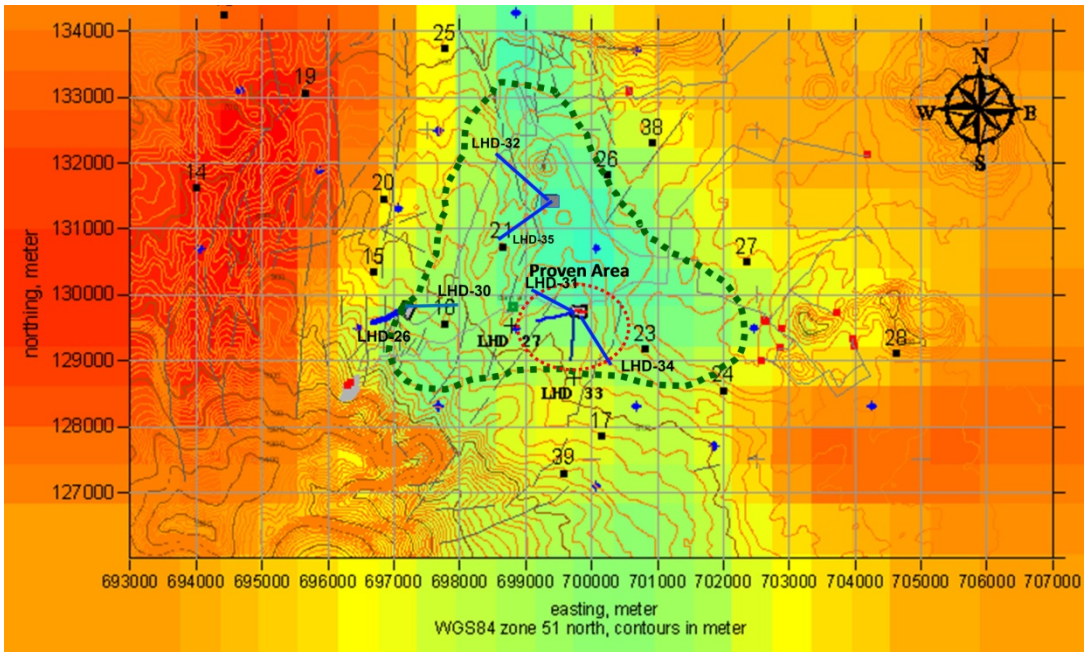

FIGURE 4: MT map of Tompaso prospects (PGE, 2008)

2.4 Downhole temperature and pressure data

Temperature and pressure of the Tompaso Geothermal field were measured and monitored using Kuster tools. In Tompaso, the current wells are divided into 3 different clusters: cluster LHD-26 (wells LHD-26 and LHD-30), cluster LHD-27 (wells LHD-27, LHD-31, LHD-33 and LHD-34) and cluster LHD-32 (wells LHD-32 and LHD-35). From temperature profiles in both LHD-26 and LHD-30 there are indications of a shallow reservoir at 400 m depth. Temperature profiles also show a distribution of high temperatures in the deep reservoir with the temperature ranging between 240 and 260°C.

The maximum temperature in cluster LHD-27 was between 240 and 260°C from 900 to 1400 m depth or 0 to 500 m b.s.l. In cluster LHD-26, maximum temperatures were between 240 and 260°C from 1600 to 1900 m depth or 800 to 1100 m b.s.l. At cluster LHD-32, the maximum temperatures measured were between 220 and 240°C from 1700 to 1800 m depth or 1000 to 1100 m b.s.l.

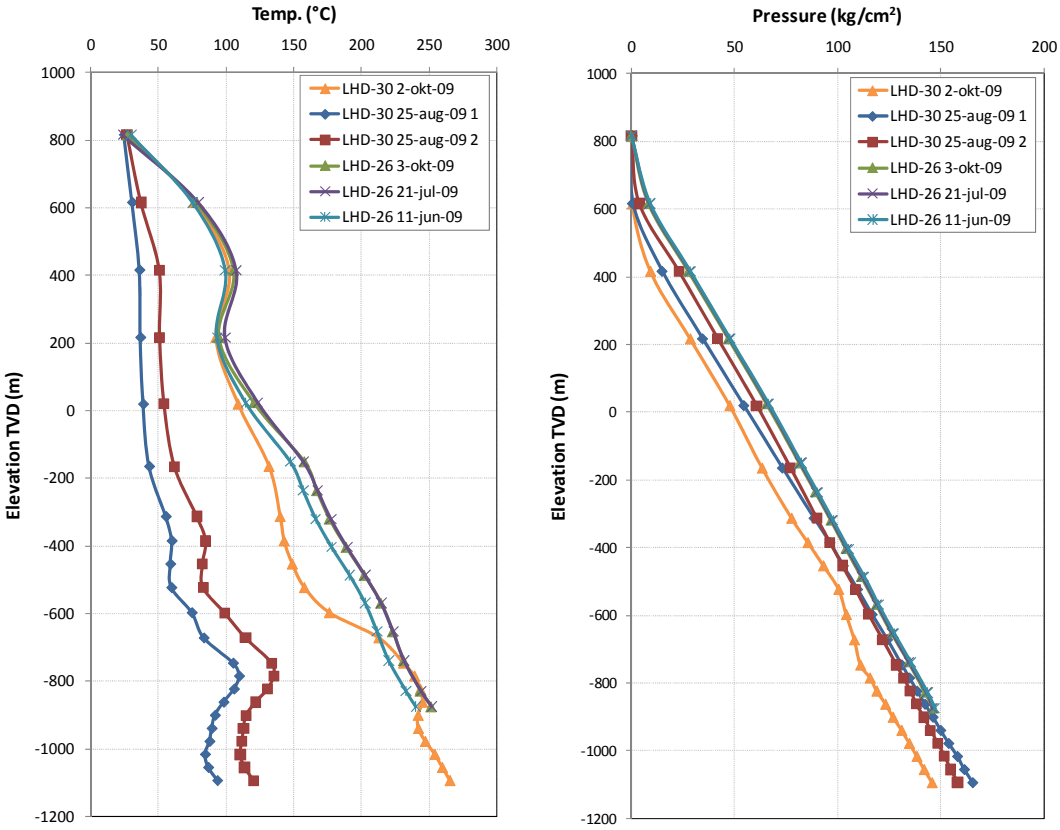

FIGURE 5: Temperature and pressure profiles for well cluster LHD-26

From the pressure profile at Tompaso it can be seen that the pressure distribution in the field is similar in all three clusters. Reservoir pressure is between 140 and 170 kg/cm^2 and the water level is at about 200 m depth. All the wells in the Tompaso field are under the saturation temperature so the fluid is in two phases. Temperature and pressure profiles for each cluster in the Tompaso geothermal field are shown in Figures 5, 6 and 7.

3. CONCEPTUAL MODEL OF TOMPASO GEOTHERMAL FIELD

Based on exploration studies including temperature and pressure measurements and well test analysis, it was determined that the main geothermal reservoir in Tompaso is located in the area around cluster-27. The top of the reservoir at cluster-27 is at 1100 m depth or 200-300 m b.s.l. At cluster-26, the shallow reservoir is located at a depth of 400 m, while the deep reservoir is at 2200 m depth or 1100-1200 m b.s.l. The estimated reservoir thickness is 400 m, from 1100 to 1500 m measured depth (1000-1400 m vertical depth). A high-permeability fracture zone was found around cluster-27 at Sendangan. The loss of circulation in this cluster is caused by faults trending NE-SW which cross the wells in this cluster (Prasetyo and Tri Handoko, 2009).

Reservoir temperature in Tompaso prospects is around 260°C, meaning that it is a liquid-dominated reservoir. Geothermal fluid chemistry is slightly acidic with a pH of 5 and low gas content (< 1% weight). Geothermal fluid moves from the upflow zone located below the Masam crater to the northeast where it flows to the surface around the Mount Tempang/Umeh area. The cap rock, which is characterised by the presence of clay minerals, is found at depths of 100-900 m or down to 100 m b.s.l. This zone is followed by a transitional zone at 900-1000 m depth (100-300 m b.s.l.) and a propylitic zone, which is the main reservoir, below 1000 m depth. The subsurface reservoir description of Tompaso field is presented in Figure 8.

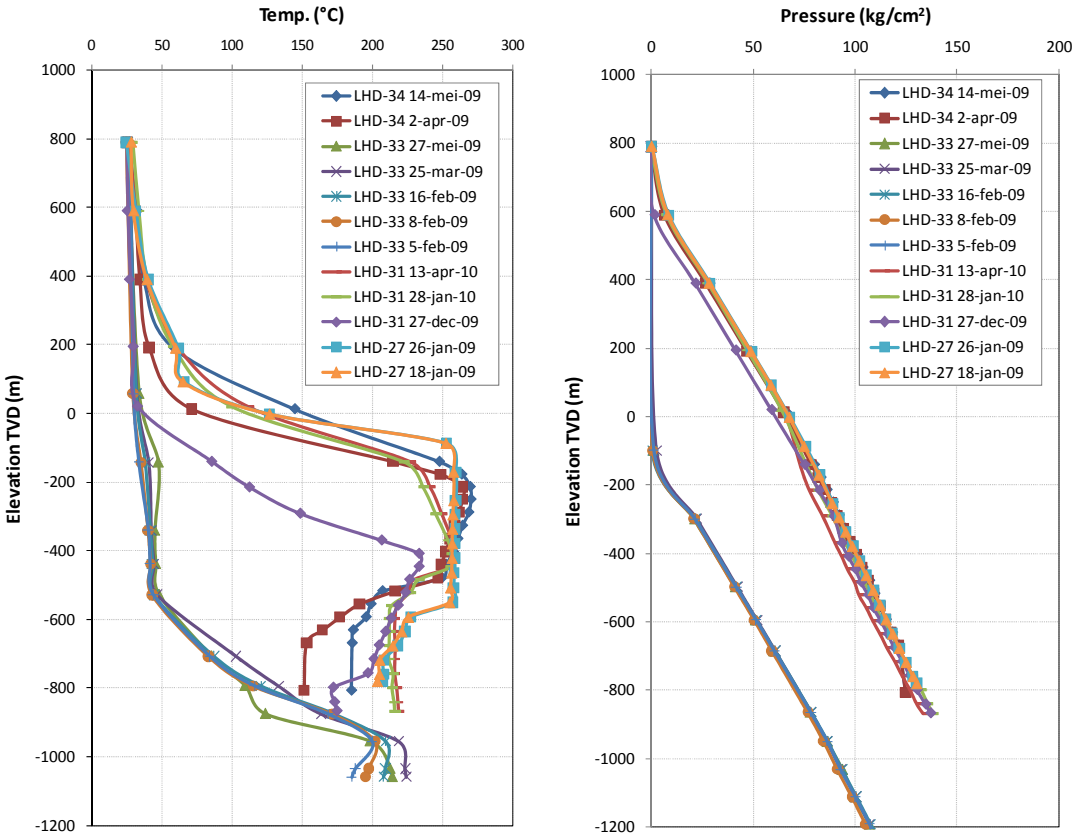

FIGURE 6: Temperature and pressure profiles for well cluster LHD-27

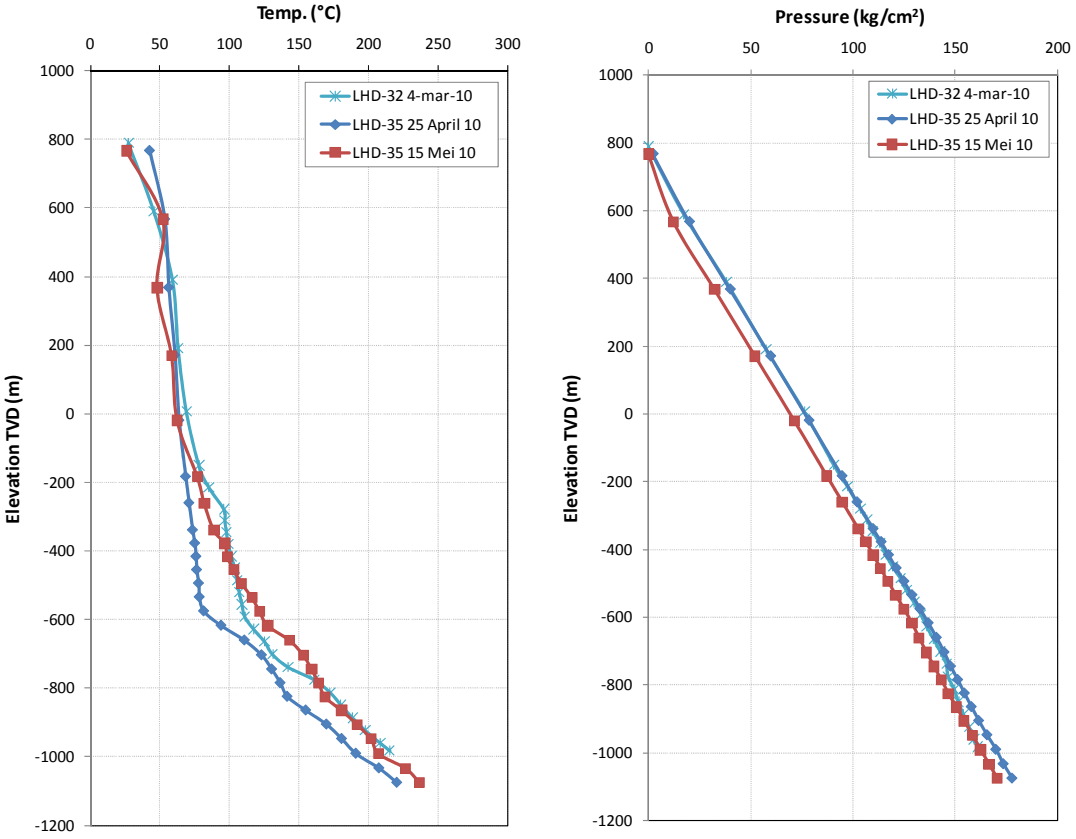

FIGURE 7: Temperature and pressure profiles for well cluster LHD-32

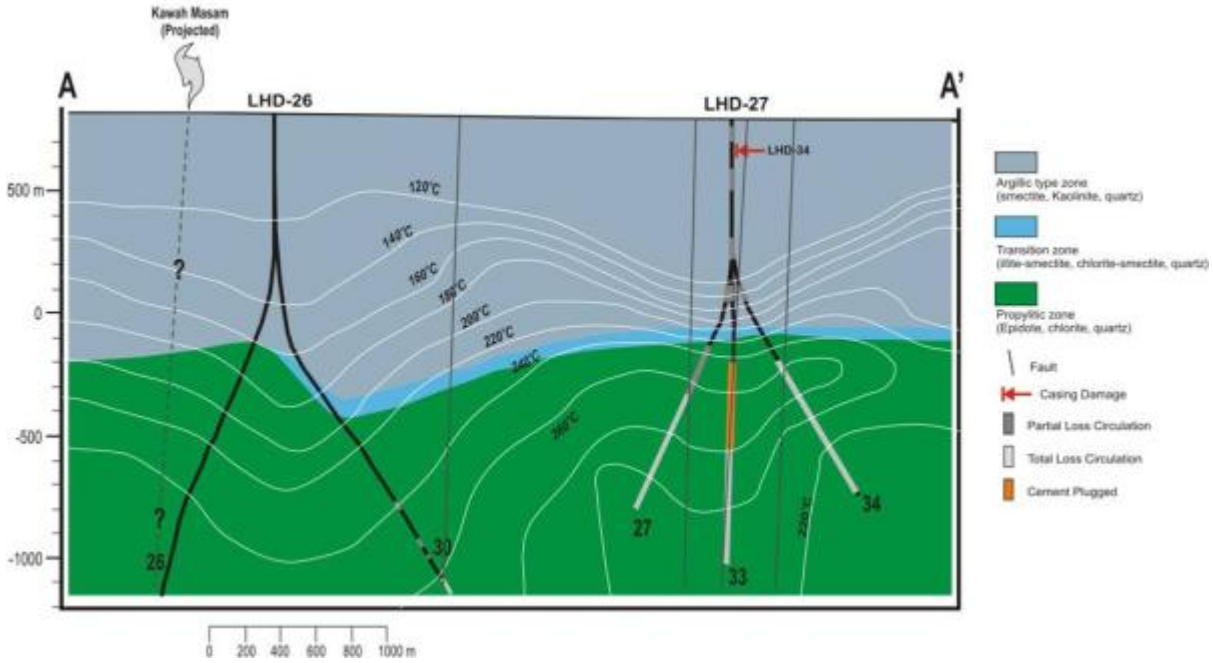

FIGURE 8: Subsurface cross-section A-A' of Tompaso wells (Prasetyo and Tri Handoko, 2009)

4. VOLUMETRIC ASSESSMENT

Volumetric models have been used internationally for decades in order to estimate the power production potential of geothermal systems. As the name indicates, the volumetric method is based on estimating the energy content of the geothermal system in question by assessing the reservoir volume and the predominant reservoir temperature above a given cut-off temperature, or rejection temperature which is based on the energy conversion technology assumed. The recoverable thermal energy is then estimated from the thermal energy available in the reservoir by using a thermal recovery factor for the producible fraction of the reservoir's thermal energy.

The volumetric method assumes that the reservoir rocks are porous and permeable and that the water mass extracted from the reservoir mines the heat from the overall volume of the reservoir. No recharge of reservoir fluids or flux of thermal energy to the reservoir volume is assumed.

4.1 The volumetric method using triangular distribution

The foundation for the volumetric method is simply to use the first law of thermodynamics to predict how much thermal energy can be recovered from a geothermal reservoir volume. The energy content (Q) stored in the geothermal reservoirs includes both the energy in the reservoir rocks and the fluid and can be estimated as:

$$Q = Ah\,(T - T_0)[(1 - \phi)C_R\rho_R + \phi C_w\rho_w] \quad (1)$$

where Q = Stored heat in the reservoir volume (J);
A = Surface area of the reservoir (m^2);
h = Reservoir thickness (m);
T = Reservoir temperature (°C);
T_o = Rejection temperature (°C);
C_R = Specific heat capacity of the rock matrix (J/kg°C);

C_W = Specific heat capacity of the reservoir fluid (J/kg°C);
ρ_R = Density of the rock matrix (kg/m^3);
ρ_W = Density of the reservoir fluid (kg/m^3); and
ϕ = Porosity of the rock matrix.

It is further assumed that the heat capacity per unit reservoir volume of the entire system is isotropic. The following equation is then used to estimate the recoverable thermal energy that can be converted to electricity, .i.e. the electrical power potential of the geothermal resource:

$$E = \frac{QR\eta F}{L} \tag{2}$$

where E = Electrical power potential (MW_e);
R = Thermal recovery factor;
η = Power plant conversion efficiency;
F = Power plant capacity; and
L = Power plant lifetime (year).

The thermal recovery factor determines the fraction of the energy that can be extracted from the reservoir rocks, and compares it to the stored energy in the reservoir. Historically, a constant recovery factor of 0.25 has been used for uniformly porous and permeable geothermal reservoirs. More recent analysis of data from fractured reservoirs indicates that the recovery factor is closer to 0.1, with a range of approximately 0.05- 0.2. In general, this apparent discrepancy in the recover factor reflects the contrast in thermal energy recovery from complex, fracture-dominated reservoirs compared to uniform, high-porosity reservoirs (Williams, 2007).

The power plant conversion efficiency describes how efficiently the recovered heat from the geothermal resource is converted to electricity. The efficiency is often taken to be 10%, but varies between power plant conversion cycles and the temperature of the resource. The thermal recovery factor, plant efficiency and reference temperature are explicit limitations set by the operational procedures, as defined by the power plant and the technique used for harnessing the heat resource.

The power plant capacity describes the plant availability, allowing for maintenance breaks and unforeseen problems related to shut-downs. For most geothermal power plants supplying base load power, this factor is usually between 90 and 95%. The power plant lifetime factor, or project lifetime, is divided by the converted electrical energy to calculate the average power plant output in MW_e. Generally the power plant lifetime factor is assumed to be 20-30 years.

4.2 Monte Carlo simulation

The Monte Carlo simulation is a repetitive calculation process stochastic model that was used in launching missile projects for the U.S. Department of Defence in the 2nd World War. The effects of subjectivity in determining the simple distribution model for each variable are reduced by using random numbers. The output from the Monte Carlo simulation calculation process is the cumulative frequency distribution that gives trust value limits (Ashat, 2009). Monte Carlo methods are a class of computational algorithms that rely on repeated random sampling to compute their results. Monte Carlo methods are often used in simulating physical and mathematical systems. Because of their reliance on repeated computations of random or pseudo-random numbers, these methods are most suited to calculation by a computer and tend to be used when it is unfeasible or impossible to compute an exact result with a deterministic algorithm.

Monte Carlo simulation methods are especially useful in studying systems with a large number of coupled degrees of freedom, such as fluids, disordered materials, strongly coupled solids, and cellular

structures. More broadly, Monte Carlo methods are useful for modelling phenomena with significant uncertainty in inputs, such as the calculation of risk in business. These methods are also widely used in mathematics; a classic use is for the evaluation of definite integrals, particularly multidimensional integrals with complicated boundary conditions. It is a widely successful method in risk analysis when compared with alternative methods or human intuition. When Monte Carlo simulations have been applied in space exploration and oil exploration, actual observations of failures, cost overruns and schedule overruns are routinely better predicted by the simulations than by human intuition or alternative soft methods.

Distribution rates
Distribution rates are a collection of observations from a price variable and are expressed in the form of a distribution frequency histogram. The histogram in Figure 9 was obtained from n times observation in the interval value Δx. The frequency per x value along interval Δx is the density of the frequency, $W(x)$ as given by:

$$W(xi) = \frac{wi}{\Delta x} \tag{3}$$

Another form of data processing observation results are cumulative frequency distributions $W(x<xi)$. The area of the distribution curve can be described by:

$$W(x < xi) = \int_{x}^{xi} w(x)dx \tag{4}$$

The maximum value of $W(x < xi) = 1$ and $W(x > xi) = 1 - W(x < xi)$.

For pressure drawdown calculations, the Monte Carlo method uses a triangular distribution (Figure 10); in a triangular distribution the observation of a variable can only be estimated in three categories (most likely, minimum and maximum). For $x \leq b$, the equation is:

$$W(x) = \frac{2(x-a)}{(b-a)(c-a)} \tag{5}$$

And for $x \geq b$, the equation is:

$$W(x) = \frac{2(c-x)}{(c-b)(c-a)} \tag{6}$$

4.3 Parameter justification for volumetric assessment

Area (A)
The size of the area is taken as the prospect area of the Tompaso geothermal field. Figure 3 is taken from the MT model of the Tompaso geothermal field, and shows the size of the prospect area. There is one well (LHD-26) outside the prospect area. The drilling data from that well reveals that there is no total loss of circulation (TLC), and only a little partial loss of circulation (PLC) which indicates that LHD-26 has limited permeability. The temperature profile shows an ambient thermal gradient along the well except between 300 and 500 mD. From Figure 3, it is assumed that the minimum area is 12 km^2 (most probably it is 16 $km^{2)}$ and the maximum area is 20 km^2.

Thickness (h)
The thickness parameter was estimated from measured temperature profiles that were measured in the field. The minimum temperature which can be used for generating electricity is around 250°C. Using the true vertical depth (TVD) temperature profiles, the minimum thickness was assumed to be 500 m, the most probable thickness 600 m and then the maximum thickness 650 m. All the thickness parameters were estimated from potential production wells.

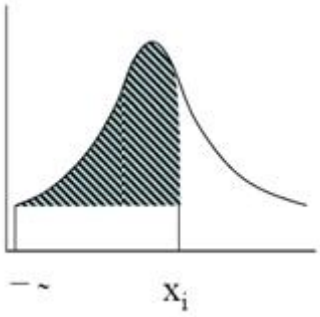

FIGURE 9: Normal distribution (Ashat, 2009)

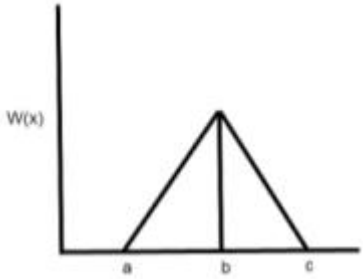

FIGURE 10: Triangular distribution (Ashat, 2009)

Porosity (ø)
The porosity value for Tompaso geothermal field was not available, so it was assumed, based on knowledge of similar geothermal systems in Indonesia. The porosity value was assumed to range between 5 and 22%, based on field data and typical rock properties (Yani, 2006).

Temperature (T)
The temperature parameter represents the temperature in the reservoir that was taken from the temperature measurements in Tompaso geothermal field (Figure 5). From the temperature measurement data, the minimum temperature is 250°C, most probable temperature 260°C, and the maximum temperature is 270°C.

Temperature cut-off (T_o)
The cut-off temperature is the temperature of the state from which the heat is integrated (Halldórsdóttir, 2010):

- The outdoor temperature;
- The minimum temperature for electricity production; and
- The minimum temperature for space heating.

From the definition, the temperature cut-off can be described as the surface temperature in Tompaso geothermal field, or the minimum temperature that can be used for electricity production. For the surface temperature, the minimum temperature cut-off is 25°C, most probably the temperature cut-off is 27°C, and the maximum temperature cut-off is 30°C.

If the temperature cut-off is the temperature for generating electricity, then the temperature for generating electricity in Lahendong geothermal field is assumed to be valid for the closest geothermal fields from Tompaso (± 30 km) while the pressure needed for the Lahendong power plant is 7-8 bars. From pressure data, the saturation temperature can be assessed by using TAFLA from the Icebox software package (Arason, et al., 2003) that was developed by ISOR. By using TAFLA, the result for the minimum temperature cut-off is 165°C (7 bars), most probably it is 168°C (7.5 bars), and the maximum temperature cut-off is 170°C (8 bars).

Specific heat capacity of the rock matrix (C_R)
From lithography logs, most of the rock in the Tompaso geothermal field is andesite and basalt rock. In *www.engineeringtoolbox.com*, there is a table that lists the specific heat capacity for a variety of rock types; from the table, the specific heat capacity for basalt rock is 0.84 kJ/kg°C or 840 J/kg°C.

Specific heat capacity of the reservoir fluid (C_w)
Using the cut-off temperature value for electrical production, the specific heat capacity of the reservoir fluid can be determined by referring to a steam table. If the minimum specific heat capacity of the

reservoir fluid is set at a value of 4351 J/kg°C (at 165°C), then the most probable value is 4361 J/kg°C (at 168°C) and the maximum value for specific heat capacity of the reservoir fluid is 4368 J/kg°C (at 170°C).

Density of the rock matrix (ρ_R)
For the density of the rock matrix, the values for andesite and basalt rock were taken from *http://geology.about.com/cs/rock_types/a/aarockspecgrav.htm,* as mentioned before. Most of the rock in the Tompaso geothermal field is andesite and basalt rock. On the website, there is a table which shows the density for various different types of rock. For andesite, the density value is listed as 2.5-2.8 gr/cm^3 or 2500-2800 kg/m^3, while for basalt the density value is 2.8-3.0 gr/cm^3 or 2800-3000 kg/m^3. Using these values, the minimum value for the rock matrix density is set at 2500 kg/m^3; the most probable value is 2800 kg/m^3 and the maximum value for the density is 3000 kg/m^3.

Density of the reservoir fluid (ρw)
Density of the reservoir fluid can be found from the cut-off temperature by using the TAFLA program (Arason, et al., 2003). From the minimum cut-off temperature, the maximum value of the fluid density is 902.3 kg/m^3; the most probable value is 899.3 kg/m^3 and the minimum value is 897.3 kg/m^3.

Power plant conversion efficiency (η)
From the lecture on volumetric assessment of geothermal fields given by Halldórsdóttir (2010) from ISOR, the mean electric conversion coefficient depends on the power plant but it can be estimated from the cut-off temperature chosen, according to:

- 150°C 11%;
- 170°C 12%;
- 180°C 13%.

If the cut-off temperature for electricity production in Lahendong power plant was such that the minimum cut-off temperature was 166°C and the maximum cut-off temperature was 170°C, then the value for the power plant conversion efficiency (η) is 12%, or more correctly, 0.12.

TABLE 1: Parameter values for volumetric assessment

Parameter	Unit	Min.	Most probable	Max.
A	km^2	12	16	20
h	m	500	600	650
T	°C	250	260	270
T_o	°C	165	168	170
C_R	J/kg°C		840	
C_{ow}	J/kg°C	4351	4361	4368
ρ_R	kg/m^3	2500	2800	3000
ρ_W	kg/m^3	902.3	899.3	897.3
ø		0.05	0.1	0.2
R		0.05	0.15	0.2
η			0.12	
F			0.95	
L	Years	20	25	30

The estimated values for the volumetric assessment are summarised in Table 1.

4.4 Volumetric assessment of Tompaso

The volumetric assessment of Tompaso geothermal field was calculated using the Monte Carlo method for three different lifetime scenarios, i.e. 20, 25 and 30 years of power plant lifetime. The results of the Monte Carlo calculations are shown in Table 2 and the example for the distribution result for 30 years of production time is shown in Figure 11.

TABLE 2: Results of volumetric assessment

Production time (Year)	P_{10} (MW_e)	P_{50} (MW_e)	P_{90} (MW_e)
20	78	58	39
25	62	46	30
30	52	39	25

5. WELL TESTING

Hydraulic well testing consists of producing from or injecting into one or more wells at controlled rates and over periods ranging from a few hours to a few weeks and monitoring changes in pressures within the producing well itself or in nearby observation wells. It should be noted here that the same formulas apply for production and injection wells with the mass flow having a reversed sign in the equations. Geothermal well testing and analysis is more difficult than the more conventional well testing techniques of hydrology and petroleum engineering. The flow in geothermal reservoirs is generally two-phase flow under non-isothermal conditions, and methods for interpreting the data for such situations are complicated (Bodvarsson and Witherspoon, 1989).

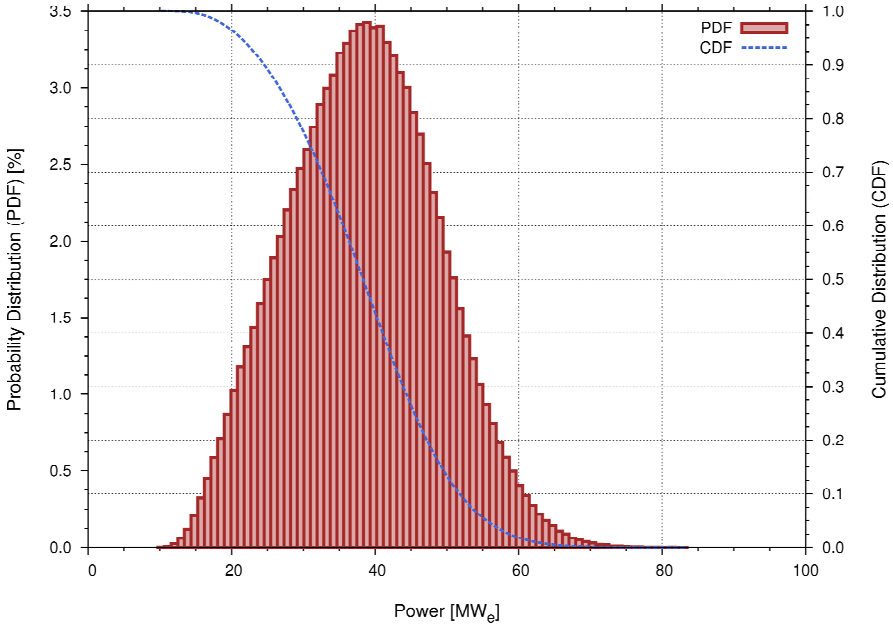

FIGURE 11: Tompaso volumetric assessment for 30 years production time scenario

5.1 Pressure transient testing

Pressure transient methods have been used for decades in evaluating groundwater and petroleum reservoirs. These methods involve creating a transient condition in the reservoir by producing from or injecting into the formation. The effects of the disturbance are then investigated by measuring the time-dependent pressure changes that occur either at the active well (single well test) or at nearby shut-in (observation) wells (interference test). The main parameters obtained from these tests are the transmissivity (*kh*) and the storativity of the reservoir region affected by the pressure transients. In the case of single well tests, one can also measure the condition of the well from the so-called "skin factor". If an indication of low permeability is found near the wellbore perhaps as the result of drilling mud invasion, the skin factor will have a large positive value (10-30). Conversely, a negative value for the skin factor is indicative of fractures that intersect the well. Other useful data can be extracted from pressure transient testing including preferential directions of permeability within the reservoir and the presence of discontinuities, such as faults.

Conventional pressure transient methods have been successfully applied to the analysis of field data from many geothermal wells, especially those completed in single-phase reservoirs. The interpretation of data from two-phase geothermal reservoirs, especially those with highly heterogeneous fracture conditions, is much more complicated and requires specialised methods of analysis.

5.1.1 Theis solution

Pressure transient tests are most often analysed using the Theis solution (Theis, 1935), which was derived for a homogeneous reservoir of uniform thickness and infinite areal extent. In this solution, it is assumed that all wells fully penetrate the reservoir so that only horizontal flow occurs and that flow

rates are constant with time. In the case of a slightly compressed fluid, such as water, the governing equation controlling the pressure response in the system is given by:

$$\frac{\partial^2 P}{\partial r^2} + \frac{1}{r}\frac{\partial P}{\partial r} = \frac{\phi \mu C}{k}\frac{\partial P}{\partial t} \tag{7}$$

For the appropriate boundary conditions and uniform initial conditions, the solution to Equation 7 is:

$$\Delta P = \frac{q\mu}{4\pi kh}\int_u^x \frac{e^{-u}}{u}\,du \tag{8}$$

where the dimensionless variable u inside the integral is given by $u = r^2/4\alpha t$. Equation 8 is often referred to as the exponential integral solution.

Although Equation 8 is based on the assumption that the well can be represented by a line source (i.e. a well of zero radius), Mueller and Witherspoon (1965) have shown that in most cases this is not a critical assumption. The effects of a producing well of finite radius are only important when observation wells are located about 5 m from the active well, which is never the case in geothermal fields.

5.1.2 Single well tests

The Theis solution can be directly applied to the analysis of downhole pressure transients from a well that is being used for production or injection at a constant rate. The exponential integral in Equation 8 can be replaced by a series solution given by:

$$\Delta P = \frac{q\mu}{4\pi kh}\left[-\gamma - \ln u + u - \frac{u^2}{2!\,2} + \frac{u^3}{3!\,3} - \ \ldots\right] \tag{9}$$

At the active well where typically $r = r_w = 0.1$ m, the dimensionless variable u decreases rapidly with time and Equation 9 can be approximated by:

$$\Delta P = \frac{q\mu}{4\pi kh}\log\frac{2.246kt}{\phi\mu C r_w^2} \tag{10}$$

The Euler's constant ($\gamma = 0.5772$) in Equation 5 has been incorporated into the log term in Equation 10. Equation 6 shows that a plot of ΔP vs. log t yields a straight line from which the reservoir parameters can be computed:

$$kh = \frac{2.303q\mu}{4\pi m} \tag{11}$$

$$øCh = \left(\frac{2.246t_0}{\mu {r_w}^2}\right)kh \tag{12}$$

where m is the pressure change per log cycle and t_o is the intercept with the time axis for zero pressure change ($\Delta P = 0$).

In geothermal systems, the thickness (h) of the reservoir is generally unknown, and hence, one can only determine the transmissivity, i.e., the permeability thickness product (kh). Also the effective porosity and the total compressibility of fluid and rock are usually not known and it is only possible to

determine the storativity (*øCh*). The effective porosity (*ø*) for fractured reservoirs represents some weighted average of the fracture porosity and the matrix porosity.

5.1.3 Interference test analysis

To analyse the pressure transient effects measured in observation wells, one must generally use the complete form of the Theis solution (Equations 8 or 9) in the analysis rather than the approximate semi-log solution (Equation 10). This type of analysis is performed using type curves that are plotted in terms of dimensionless parameters, which are defined as:

Dimensionless pressure:

$$P_D = \frac{2\pi kh}{q\mu}\Delta P \tag{13a}$$

Dimensionless time:

$$t_D = \frac{kt}{\phi\mu C r^2} \tag{13a}$$

Dimensionless distance:

$$r_D = \frac{r}{r_w} \tag{13c}$$

Using these dimensionless parameters, the Theis solution becomes:

$$P_D = \frac{1}{2}\int_{1/4t_D}^{x} \frac{e^{-y}}{y}dy = \frac{1}{2}\left[-\gamma + ln\,4t_D + \frac{1}{4t_D} - \frac{1}{2.2!\,(4t_D)^2} + \frac{1}{3.3!\,(4t_D)^3} - \cdots\right] \tag{14}$$

The relationship between P_D and t_D is readily obtained from Equation 14 and has been tabulated by Witherspoon et al. (1967).

5.1.4 Pressure build-up and fall-off tests

Analytical methods assume a constant rate of production or injection is maintained throughout the test. These methods can readily be extended to pressure build-up (after production) and fall-off (after injection) tests. To do this, the principle of superposition must be used. For example, in the case where one wants to measure the effects of pressure build-up in the active well, one mathematically treats the shut-in period when $q = 0$ as the sum of the pressure change due to continued production ($q = q_P$) and that, due to injection at the same rate ($q = -q_P$) starting at the time of shut-in:

$$\Delta P = \frac{q\mu}{4\pi kh}\left[\ln\frac{4k(t_p + \Delta t)}{\phi\mu C {r_w}^2} - \gamma\right] - \frac{q\mu}{4\pi kh}\left[\ln\frac{4k\,\Delta t}{\phi\mu C {r_w}^2} - \gamma\right] \tag{15}$$

or

$$\Delta P = \frac{q\mu}{4\pi kh\left[\ln\frac{t_p + \Delta t}{\Delta t}\right]} \tag{16}$$

where t_p is the duration of production and Δt is the elapsed time after shut-in.

The pressure build-up data can be plotted vs. log $(t_p + \Delta t)/\Delta t$ and the resulting straight line used to determine *kh* from Equation 11. Also, by extrapolating the pressure to the Horner time, when $(t_p + \Delta t)/\Delta t \rightarrow 1$ (Horner, 1951), one can obtain an estimate of the reservoir pressure. And for skin factor, the equation can be derived as:

$$P_{skin} = 1.15 \left[\frac{P_{1hr} - P_i}{m} - log\left(\frac{k}{\mu\phi C_t {r_w}^2}\right) - 3.91\right] \quad (17)$$

where P_{skin} is the skin factor from the well and *m* is the slope which is obtained from extrapolating pressure to the Horner time; *k* is the permeability value that is obtained from Equation 11 by dividing permeability thickness with the reservoir thickness.

This should be the original reservoir pressure provided the system acts as if it were of infinite areal extent. If the system is bounded or other wells are being produced, the extrapolation of the pressure data will yield an estimate for the pressure drawdown.

5.1.5 Multi-rate tests

Multi-rate tests are often employed in geothermal wells, especially step-rate injection tests at the end of drilling. These tests typically consist of three to five steps, each with a constant rate, followed by a pressure fall-off (Figure 12). The injection rate is often increased during such a test up to the maximum injectivity of the well, if sufficient water is available. For a typical geothermal well with a 0.1 m well radius in the open interval, the length of each step should exceed 3 hours in order to obtain data without significant wellbore storage effects. Such tests can be analysed using the proper superposition of the Theis solution (Matthews and Russell, 1967; Earlougher, 1977) and the log-approximation for the active well. For a multi-rate flow test with n steps of duration $t_1, t_2 \ldots t_n$ and rates of $q_1, q_2 \ldots q_n$, the pressure drop is given by:

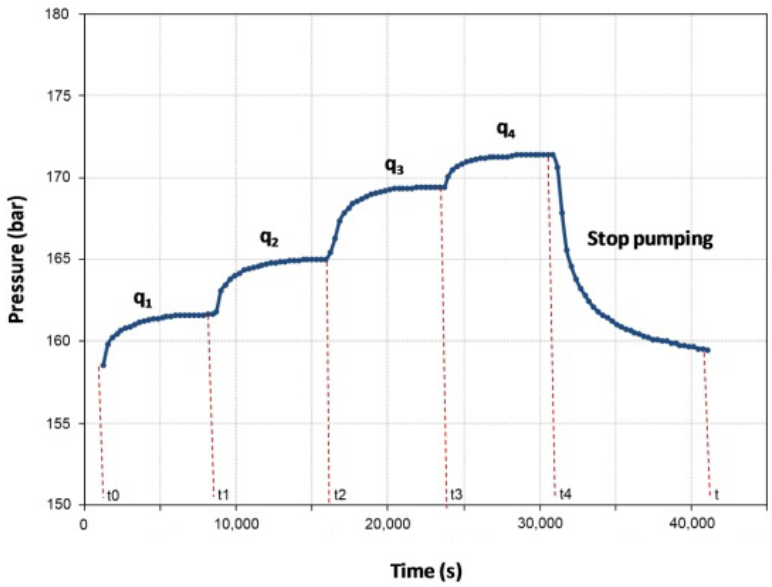

FIGURE 12: Example of well test data

$$\Delta P = \frac{\mu}{2\pi kh} \sum_{i=1} \Delta q_i \left[\frac{1}{2} W\left(\frac{{r_w}^2 S}{4T(t - t_i)}\right) + P_{skin}\right] \quad (18)$$

where

$$W(u) = \int_u^{\infty} \frac{e^{-u}}{u} du \quad (19)$$

The explanation for well function or *W(u)* will be discussed later in this report.

5.2 Aquifer properties

Aquifer properties are, of course, defined when rock and fluid properties are separately defined. But in the literature several parameters are defined which are combined quantities. Those discussed here are the storage coefficient (*S*) and transmissivity (*T*).

Storage coefficient (S)
Storage coefficient is defined as the volume of water released by unit volume of reservoir for unit drop in pressure head. The storage coefficients are very different for single-phase and two-phase reservoirs. Storage coefficient can be defined as:

$$S = C_t \, h \, \rho \, g \tag{20}$$

where S = Storativity (dimensionless);
h = Thickness (m);
C_t = Total compressibility (1/Pa); $C_t = \phi \, C_w + (1 - \phi) \, C_r$; and
g = Gravity (9.81 m/s^2).

Transmissivity (T)
The transmissivity is a measure of how much water can be transmitted horizontally, such as to a pumping well, so that transmissivity of an aquifer can be determined from pumping tests.
Transmissivity is usually denoted by *T* and is defined as:

$$T = Kh \tag{21}$$

where *K* is the coefficient of permeability and has the dimension of velocity.

The coefficient of permeability, *k*, depends on the viscosity and density of the fluid and geometrical properties of the rock. Like viscosity, the coefficient of permeability is also very temperature dependent. Another coefficient of permeability, which is independent of fluid properties, is the intrinsic permeability (*k*) defined as:

$$k = \frac{\mu}{\rho g} K \tag{22}$$

where T = Transmissivity (m^2/s);
k = Permeability (m^2);
h = Thickness (m);
μ = Dynamic viscosity of the fluid (Pas);
ρ = Density of the fluid (kg/m^3); and
g = Gravity (9.81 m/s^2).

5.3 Well function approximation for confined aquifers

Pumping tests are commonly used to determine the transmissivity and storage coefficients of a confined aquifer. Computation of the Theis well function (1935) is an essential part of this process. Most early investigations involved reading the value of the well function from a table, using an approximation valid for small values of the argument or using numerical integration. An analytical expression for the drawdown in an observation well located at a distance *r* from the pumping well, assuming a homogeneous and isotropic aquifer with a uniform thickness and infinite areal extent, was presented by Theis (1935):

$$\Delta P = \frac{g}{2\pi T}\sum_{i=1}\Delta q_i \left[\frac{1}{2}\, W\left(\frac{{r_w}^2 s}{4T(t-t_i)}\right) + P_{skin}\right] \tag{23}$$

where ΔP = Drawdown pressure (Pa);
q = Constant pumping rate (kg/s);
T = Transmissivity (m^2/s);
h = Thickness (m);
s = Storativity;
P_{skin} = Skin factor;
t = Pumping time (s);
r_w = Radius of the well (m); and
$W(u)$ = Well function.

The dimensionless parameter u, which depends on time t, is defined as:

$$u = \frac{r^2 S}{4Tt} \tag{24}$$

where S = Storage coefficient.

$W(u)$ is the well function defined by an infinite series as:

$$W(u) = \int_u^{\infty} \frac{e^{-u}}{u} du = -0.5772 - \ln u + \sum_{i=1}^{\omega} \frac{u^i}{i\ x\ i!} \tag{25}$$

Since the well function is an integral function of S and T, it is not possible to determine explicitly the aquifer parameter S and T from a set of values of s and t in an observation well. For practical purposes, the simplest was proposed by Cooper and Jocob (1946) for $u < 0.05$, thus:

$$W(u) = -0.5772 - \ln u \tag{26}$$

Swamee and Ojha (1990) proposed an approximation for the well function, valid in the full range:

$$W(u) = \left(\left[\left(\frac{0.56146}{u} + 0.65\right)(1+u)\right]^{-7.7} + u^4 e^{7.7u}(2+u)^{3.7}\right)^{-0.13} \tag{27}$$

Srivastava (1995) concluded that the approximate expression given by Equation 22 is less accurate and more computationally intensive than those given in Equation 26. Srivastava (1998) based on the slope-matching technique, proposed the more accurate and less computationally intensive approximations given by the following:

For $u \leq 1$:

$$W(u) = \ln\left(\frac{C_1}{u}\right) + 0.9563u - 0.1690u^2 \tag{28}$$

For $u \geq 1$:

$$W(u) = \frac{1}{ue^u}\frac{u + 0.3575}{u + 1.280} \tag{29}$$

For our case, Equation 27 is used for calculating the well function, as there are no limitations for Equation 27 and we can calculate continuously to find the u value.

5.4 Well test results

A completion test consists of pressure and temperature measurements, a water loss test and a gross permeability test. In Tompaso, not all of the wells got a completion test, only wells LHD-30, 31, 32, 34 and 35 (Tri Handoko, 2009a, b, c, and 2010; Prabowo and Prasetyo, 2010). The whole completion test takes about 36 hours. For the gross permeability test, the test consisted of four different pumping rates (step test) to measure the pressure build-up of the well, after which pumping was stopped and the well was observed for the fall-off test.

The objective of a gross permeability test is to find the transmissivity value or permeability thickness and storativity. For our case, we wanted to make a match between measured data and calculated data taken from the gross permeability test.

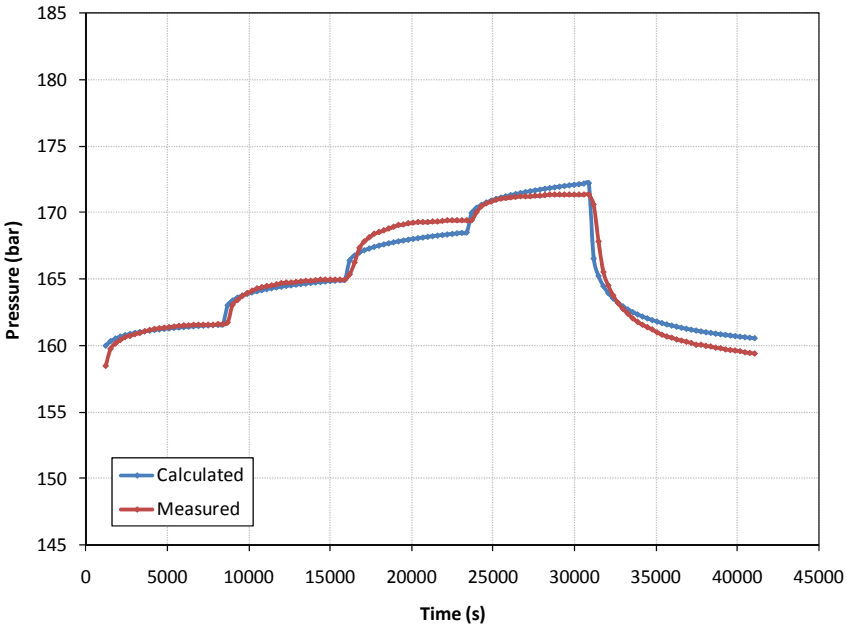

FIGURE 13: Pressure vs. time LHD-30

LHD-30

The gross permeability test for well LHD-30 used 4 different pumping rates to evaluate the pressure build-up in the well (Figure 13). The water was pumped into the well using 1000, 2000, 3000 and 4000 l/min. pumping rates for 2 hours each. Afterwards, pumping was stopped and the pressure was analysed for the fall-off test using the Horner plot (Figure 14). From matching the measured data and the calculated data from well LHD-30, the values of transmissivity, storativity and skin effect were found. For well LHD-30, the value of transmissivity = 2.55×10^{-3} m^2/s, storativity = 12.70 and the skin effect = -0.01.

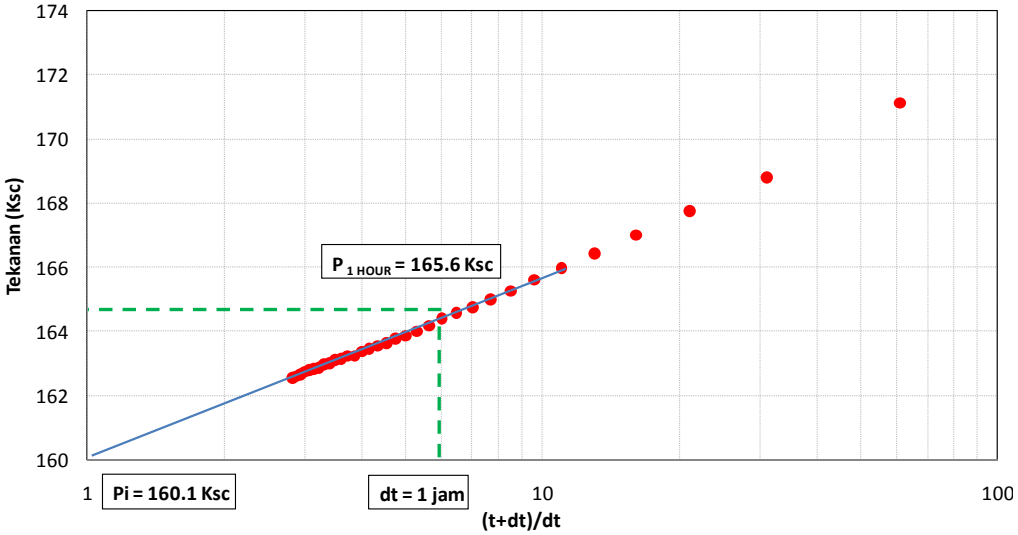

FIGURE 14: Horner plot graph from fall-off test LHD-30

HD-31

In well LHD-31, the injected water for the gross permeability test used pumping rates of 1000, 2000,

3000 and 4000 l/min. for 2 hours each. Then, pumping was stopped for the fall-off test. For well LHD-31, the calculated data values were: transmissivity = 1.60×10^{-2} m^2/s, storativity = 1.07×10^{-3} and the skin = -0.52.

LHD-32
For well LHD-32, the injected water pumping rates used for the gross permeability test were 1000, 2000, 3000 and 4000 l/min. for 2 hours each. Then, pumping was stopped for the fall-off test. From matching the measured data and the calculated data of well LHD-32, the following values were calculated: transmissivity = 2.40×10^{-3} m^2/s, storativity = 4.30×10^{-2} and the skin = -0.24.

LHD-34
The gross permeability test for well LHD-34 used 4 different pumping rates to find the pressure build-up in the well. The pumping rates into the well were 1000, 2000, 3000 and 4000 l/min., for 2 hours each. Afterwards, pumping was stopped and the pressure was analysed for the fall-off test. For well LHD-34, the calculated values were: transmissivity = 7.63×10^{-2} m^2/s, storativity = 1.56×10^{-4} and the skin = -2.65.

LHD-35
For well LHD-35, the pumping rates for the injected water used for the gross permeability test, were 1000, 1100, 1200 and 1300 l/min., for 2 hours each. Then pumping was stopped for the fall-off test. For well LHD-35, the calculated values were: transmissivity = 3.78×10^{-4} m^2/s, storativity = 5.84×10^{-3} and the skin = -0.48.

After calculating the transmissivity, storativity and skin values, using all the data from the gross permeability test, it can be seen that the values are different from the values calculated using only fall-off test data. The comparison between using all the gross permeability data (step test) and based on only the fall-off test data is shown in Table 3.

TABLE 3: Comparison between step test and fall-off test values

Well	Fall-off test			Step test		
	Transmissivity (m^2/s)	Storativity	Skin	Transmissivity (m^2/s)	Storativity	Skin
LHD-30	2.07×10^{-4}	1.57×10^{-4}	-0.04	2.55×10^{-3}	1.27×10^{1}	-0.01
LHD-31	5.03×10^{-4}	5.37×10^{-4}	-1.67	1.60×10^{-2}	1.07×10^{-3}	-0.52
LHD-32	6.02×10^{-5}	1.68×10^{-4}	-0.82	2.40×10^{-3}	4.30×10^{-2}	-0.24
LHD-34	6.78×10^{-4}	6.73×10^{-4}	-2.34	7.63×10^{-2}	1.56×10^{-4}	-2.65
LHD-35	1.58×10^{-5}	1.75×10^{-4}	-0.58	3.78×10^{-4}	5.84×10^{-3}	-0.48

From Table 3 it can be seen that the values for transmissivity, storativity and skin from both tests are different. This happens because the values were calculated from 2 different conditions. From the fall-off test, we got transmissivity, storativity and skin values for the condition in which pumping had stopped and the water level had started to return to its initial state. While from the step test, we calculated transmissivity, storativity and skin value from all the test data, from when the well was injected with water at different pumping rates as well as when pumping had stopped. Most of the data were calculated in the pumping condition and then the water level of the wells increased. Thus, very different values for transmissivity, storativity and skin were obtained from these tests.

The storativity values in LHD-30 were different because of the different temperatures in the well when the well tests were being implemented. The maximum temperature that was measured in LHD-30 before the well test was implemented was 135.11°C; the maximum temperatures measured in other wells before the well test were < 200°C.

6. PRESSURE DECLINE

6.1 Theoretical background

Pressure decline analysis is concerned with the manner by which the production of a single well or a group of wells declines with time. If an appropriate decline curve can be found that fits the data satisfactorily, one would have a way of predicting future production rates (Zais and Bodvarsson, 1980). The predicted well production rates could then be used to estimate the constant rate of energy extraction. Various functional forms have been suggested in pressure decline curve analysis where the production data was said to follow the exponential, hyperbolic or harmonic forms of decline (Arps, 1945; Fetkovich, 1980). The decline curve method of analysis has been used with some success in evaluating reserves for vapour-dominated geothermal systems (Budd, 1972; Dykstra, 1981; Drenick, 1988), but much less experience is available in dealing with hot water reservoirs.

The semi steady-state or pseudo steady-state solutions occur when the pressure decline is proportional to time. This means that the pressure decline curve has struck impermeable boundaries all around the producing well and the reservoir is being depleted at a constant rate. Using the storage coefficient in Equation 20, the equation will be:

$$A(dp)c\phi h\gamma = -q(dt)g \tag{30}$$

where A is the drainage area.

Or:

$$\frac{dp}{dt} = -\frac{q}{c\phi h\rho A} \tag{31}$$

If we have a circular drainage area with drainage radius, r_e then the equation will be:

$$\frac{dp}{dt} = -\frac{q}{c\phi h\rho\pi r_e^2} \tag{32}$$

In the case of liquid-dominated reservoirs with isothermal flow, the term $\frac{\partial}{\partial r}\left(\frac{k}{\mu}\right) = 0$, and if we assume that the pressure gradients are small, then terms of the order $(\partial p/\partial r)^2$ can be neglected. Then, Equation 7 will be:

$$\frac{1}{r}\frac{\partial}{\partial r}\left(r\frac{\partial p}{\partial r}\right) = \frac{\phi\mu c}{k}\frac{\partial p}{\partial t} \tag{33}$$

Using Equations 32 and 33, then:

$$\frac{1}{r}\frac{\partial}{\partial r}\left(r\frac{\partial p}{\partial r}\right) = -\frac{q\mu}{h\rho k\pi {r_e}^2} \tag{34}$$

And when this equation is integrated, it gives:

$$r\frac{\partial p}{\partial r} = -\frac{q\mu r^2}{2\pi {r_e}^2 kh\rho} + C \tag{35}$$

where C is a constant of integration.

At the outer, no-flow boundary $\partial p/\partial r$ vanishes and, hence, the constant can be evaluated as $C = \frac{q\mu}{2\pi kh\rho}$ which, when substituted into the last equation, gives:

$$\frac{\partial p}{\partial r} = \frac{q\mu}{2\pi kh\rho}\left(\frac{1}{r} - \frac{r}{{r_e}^2}\right) \tag{36}$$

Integrating once again:

$$P_r - P_{wf} = \frac{q\mu}{2\pi kh\rho}\left(\ln\frac{r}{r_w} - \frac{r^2}{2{r_e}^2}\right) \tag{37}$$

in which the term $r^2/2{r_e}^2$ is considered negligible.

Equation 33 is a general expression for pressure as a function of the radius. In this particular case when $r = r_e$ then:

$$P_e - P_{wf} = \frac{q\mu}{2\pi kh\rho}\left(\ln\frac{r_e}{r_w} - \frac{1}{2}\right) \tag{38}$$

Figure 15 shows the pressure distribution after the well has been producing at a constant rate for some time *t*. The mass balance equation for the drainage volume is given by:

$$\int_{r_w}^{r_e} (P_i - P_r)\, 2\pi r dr c\phi h\rho = qt \tag{39}$$

which can be simplified as:

$$P_i Ac\phi h\rho - \int_{r_w}^{r_e} P_r 2\pi r c\phi h\rho dr = qt \tag{40}$$

Inserting Equation 40 for P_r gives:

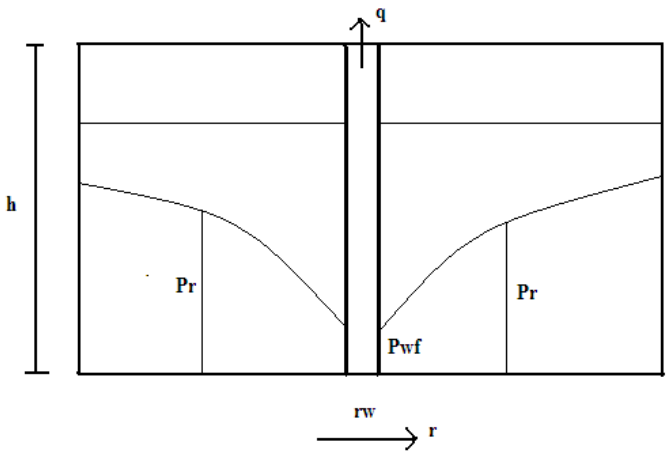

FIGURE 15: Pressure distribution for the solution of the radial diffusivity equation under semi-steady state conditions (Kjaran and Elíasson, 1983)

$$P_i Ac\phi h\rho - P_{wf} Ac\phi h\rho + P_{wf}\pi {r_w}^2 c\phi h\rho - \frac{q\mu c\phi}{k}\int_{r_w}^{r_e} r\left(ln\frac{r}{r_w} - \frac{r^2}{2{r_e}^2}\right)dr = qt \quad (41)$$

As $\pi {r_w}^2 < A$ this equation can be approximated by:

$$(P_i - P_{wf})Ac\phi h\rho - \frac{q\mu c\phi}{k}\int_{r_w}^{r_e} r\left(ln\frac{r}{r_w} - \frac{r^2}{2{r_e}^2}\right)dr = qt \quad (42)$$

Integrating Equation 42 gives approximately:

$$(P_i - P_{wf})Ac\phi h\rho - \frac{q\mu c\phi}{k} A\left(\frac{1}{2} ln\frac{r_e}{r_w} - \frac{3}{8}\right) = qt \quad (43)$$

which can be written as:

$$P_{wf} = P_i - \frac{q\mu}{2\pi k\rho h}\left(\ln\frac{r_e}{r_w} - \frac{3}{4} + \frac{kt2\pi}{Ac\phi\mu}\right) \quad (44)$$

Equation 44 is identical to Equation 38 except that it is expressed in initial pressure, P_i instead of boundary pressure, P_e. Equation 44 can be written as:

$$P_{wf} = P_i - \frac{q\mu}{2\pi k\rho h}\left(\frac{1}{2}\ln\frac{4A}{K\, C_A {r_w}^2} + 2\pi\frac{kt}{Ac\phi\mu}\right) \quad (45)$$

where K is the exponential of Euler's constant and A is the drainage area, equal to $\pi {r_e}^2$ and C_A is called the drainage shape factor.

Equation 46 was derived by circular geometry, resulting in factor C_A = 31.6. Using Equations 20 and 21 to put transmissivity and storativity values into Equation 45, the equation will be derived as:

$$P_{wf} = P_i - \frac{qg}{2\pi T}\left(\frac{1}{2}\ln\frac{4A}{K\, C_A {r_w}^2} + 2\pi\frac{Tt}{AS}\right) \quad (46)$$

where P_{wf} = Bottom hole flowing pressure (Pa);
P_i = Initial pressure (Pa);
q = Production flow rate (kg/s);
K = Euler's constant;
C_A = Drainage shape factor;
r_w = Wellbore radius (m); and
t = Time (second).

Then Equation 46 is used to calculate the pressure drawdown in Tompaso geothermal field for certain production time scenarios.

6.2 Pressure drawdown

By using Equation 44 and allowing for some of the input parameters to be assigned randomly (Monte Carlo method), the rate of pressure drawdown can be calculated. Allowing for the parameters to be set randomly accounts for some the uncertainty in this methodology. Using triangular distribution from

the Monte Carlo method with 10,000 sample values, pressure drawdown was calculated, and standard deviation was used for the error bars of the decline rate.

If it is assumed that the area influenced by production pressure drawdown is about 150 km^2, with a production rate of about 550 ton/hour (40 MW_e) for a 30 year production scenario, using the transmissivity and storativity values that were calculated from well testing, then the pressure drawdown results can be found. The values that were used to calculate the pressure drawdown are listed in Table 4.

TABLE 4: Properties for pressure drawdown calculation

Parameter	Unit	Min.	Max.	Most likely
P_i	kg/cm^2	-	-	135.48
q	ton/hour	500	600	550
	kg/s	138.89	166.67	152.78
g	m/s^2			9.81
T	m^2/s	3.78×10^{-4}	7.64×10^{-2}	1.95×10^{-2}
A	km^2	140	150	145
K		-	-	1.781
C_A		-	-	31.6
r_W	m	-	-	5000
t	year	-	-	30
S		1.07×10^{-3}	5.84×10^{-3}	3.46×10^{-3}

The histogram of frequency vs. ΔP taken from the Monte Carlo calculation for 15 years is shown in Figure 16 and the results for pressure drawdown, using 550 ton/hour production rate for a 30 year scenario, are shown in Figure 17.

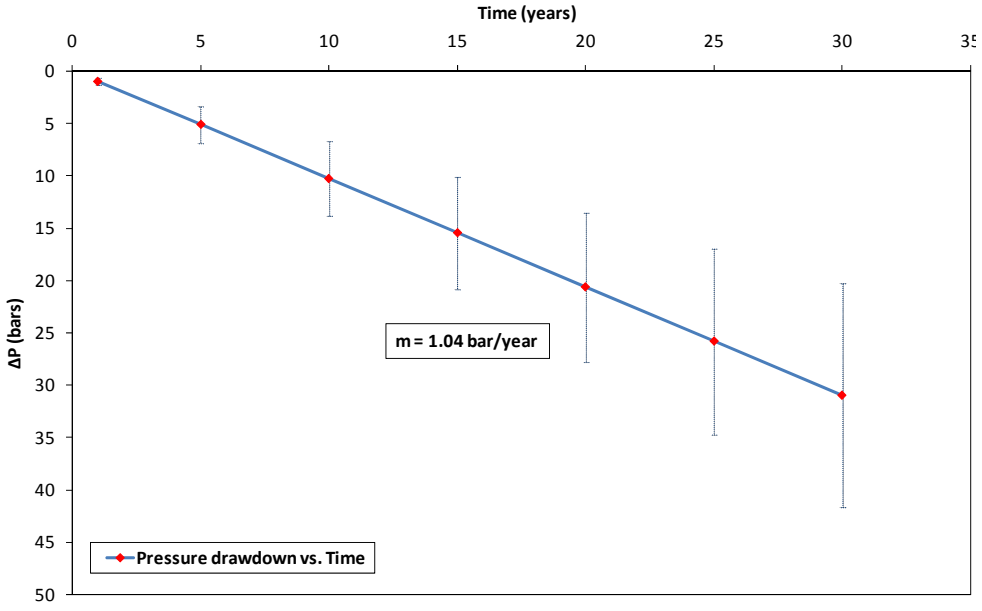

FIGURE 16: Frequency histogram of ΔP based on Monte Carlo calculations with 550 ton/hour production rate in 15 years

The rate of decline can be derived from the pressure drawdown results. The decline rate for Tompaso geothermal field is shown in Table 5.

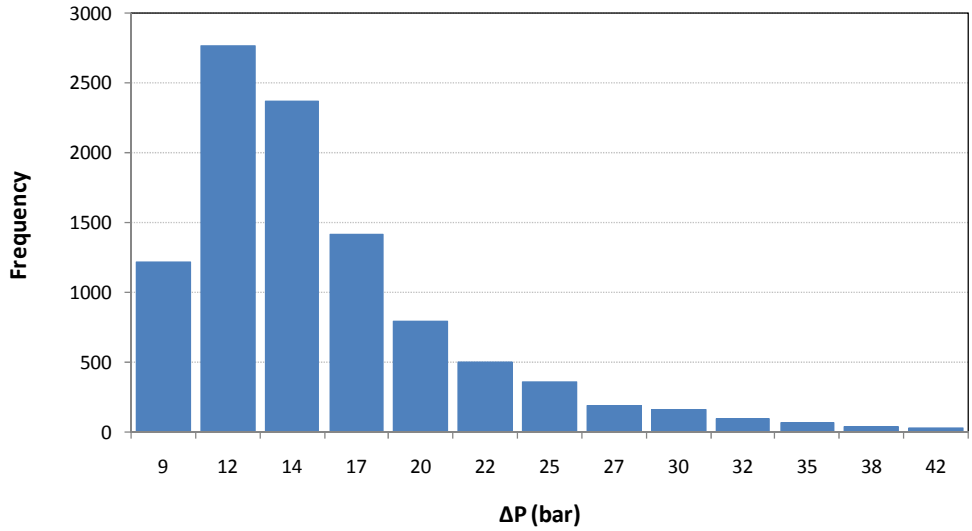

FIGURE 17: Pressure drawdown for 550 ton/hour production rate

TABLE 5: Pressure drawdown calculation results

Production (Ton/hour)	Decline rate (bar/year)	
	Average	Std. deviation
500	0.94	0.34
550	1.04	0.36
600	1.13	0.39

7. CONCLUSIONS AND RECOMENDATIONS

This paper discusses the use of volumetric estimations, well testing and pressure decline calculations for the Tompaso geothermal field. The volumetric assessment was used to estimate the available power for different production time scenarios (20, 25 and 30 years) by using the Monte Carlo method. Well test analysis was used on step build-up tests to calculate the values of transmissivity, storativity (aquifer properties) and skin effects (well property). These parameters were then compared to previous values obtained from the analysis of a fall-off test. Lastly, pressure decline calculations were performed assuming a 30 year production time and production of 40 MW_e.

7.1 Conclusions

- From the volumetric assessment, assuming a 25 year production scenario, the calculations show an electrical power potential range of:

  P_{10} = 71 MW_e, P_{50} = 51 MW_e P_{90} = 33 MW_e

- From the well test analysis of both fall-off tests and step build-up tests, values of transmissivity, storativity and skin effects were estimated for each well in the Tompaso geothermal field.

- Using the estimated transmissivity and storativity, the average decline rate in reservoir pressure was calculated to be between 0.95 and 1.13 bar/year, assuming a steady production of 40 MW_e over 30 years.

7.2 Recommendations

- Reservoir monitoring is needed during the production phase in Tompaso. It will be used for calibrating and improving the volumetric assessment and pressure drawdown simulations.

- Better well testing is recommended, with testing over a longer time interval in order for the reservoir to reach a stable condition. Also, better measurement tools would improve the accuracy of the well test data.

- The pressure drawdown results can be used for a comparative study of different production scenarios in order to determine the optimum production scenario for the Tompaso geothermal field.

ACKNOWLEDGEMENTS

I would like to express my gratitude to all the UNU-GTP staff, Dr. Ingvar B. Fridleifsson, Mr. Lúdvík S. Georgsson, Ms.Thórhildur Ísberg, Ms. Dorthe H. Holm, Mr. Markús A.G. Wilde and Mr. Ingimar G. Haraldsson for their care, generous help, advice and assistance. And I am very grateful to the UNU, PT. Pertamina Geothermal Energy and the Government of Iceland for giving me this opportunity to improve my knowledge and skills with this UNU Geothermal Training Programme Fellowship.

I am sincerely thankful to my supervisors, Dr. Andri Arnaldsson and Dr. Snorri Páll Kjaran from Vatnaskil Engineers for their time, guidance and support during project execution. Also, special thanks to the entire reservoir engineering group for sharing their knowledge and expertise with me.

REFERENCES

Arason, Th., Bjornsson, G., Axelsson, G., Bjarnason, J.Ö., and Helgason, P., 2003: *The geothermal reservoir engineering software package Icebox, user's manual*. Orkustofnun, Reykjavik, manual, 53 pp.

Arps, J.N., 1945: *Analysis of decline curves*. Trans, AIME.

Ashat, A., 2009: *Monte Carlo simulation*. Training advanced geothermal reservoir engineering, Bandung, Indonesia, unpublished lecture notes.

Bodvarsson, G.S., and Witherspoon, P.A., 1989: Geothermal reservoir engineering part 1. *Geotherm. Sci & Tech*., 2, 1-68.

Budd, C.F., 1972: *Producing geothermal steam at the Geysers field.* SPE paper 4178, Bakersfield, California.

Cooper, H.H. Jr., and Jocob, C.E., 1946: A generalized graphical method for evaluation formation constants and summarizing well-field history. *American Geophysical Union, Trans., 27*, 526-534.

Drenick, A., 1988: Reservoir development strategy for vapor-dominated geothermal reservoirs. *Geothermal Resources Council Bulletin, 17-3,* 55-68.

Dykstra, H., 1981: *Reservoir assessment of the Geyser geothermal field, California*. Div. Oil and Gas, Sacramento, California.

Earlougher, R.C., 1977: *Advances in well test analysis.* SPE monograph No.5, 264 pp.

Fetkovich, M.J., 1980: Decline curve analysis using type curves. *J. Petrol. Technol., 32-7*, 1067-1077.

Halldórsdóttir, S., 2010: *Volumetric assessment of geothermal fields*. UNU-GTP, Iceland, unpublished lecture notes.

Horner, D.R., 1951: Pressure buildup in wells. *Proceedings 3rd World Petroleum Congress, The Hague, 2*, 503-523.

Kjaran, S.P., and Elíasson, J., 1983: *Geothermal reservoir engineering lecture notes*. UNU-GTP, Iceland, report 2, 250 pp.

Matthews, C.S., and Russel, R.G., 1967: *Pressure buildup and flow tests in wells*. SPE monograph No.1, 25 pp.

Mueller, T.D., and Witherspoon, P.A., 1965: Pressure interference effects within reservoirs and aquifers. *J. Petrol. Technol., 17*, 471-474.

PGE, 2008: *Drilling prognosis well LHD-26 until LHD-34*. PT. Pertamina Geothermal Energy, Engineering Lahendong area and PSD, internal report.

Prabowo, T., and Prasetyo, I.M., 2010: *Well completion test report LHD-35*. PT. Pertamina Geothermal Energy, Indonesia, internal report.

Prasetyo, I.M., and Tri Handoko, B., 2009: *Model and reservoir characterization of Tompaso geothermal field*. PT. Pertamina Geothermal Energy, Indonesia, internal report.

Srivastava, R., 1995: Implications of using approximate expressions for well function. *J. Irrig. and Drain Engineering, 121-6*, 459-462.

Srivastava, R., 1998: Practical approximations of the well function. *Ground Water, 36-5,* 844-848.

Swamee, P.K., and Ojha, C.S.P., 1990: Pump test analysis of confined aquifer. *J. Irrig. and Drain. Engineering, 116-1*, 66-106.

Theis, C.V., 1935: The relation between the lowering of Piezometric surface and the rate and duration of discharge of a well using groundwater storage. *American Geophysical Union, Trans., 16*, 519-524.

Tri Handoko, B., 2009a: *Well completion test report LHD-30*. PT. Pertamina Geothermal Energy, Indonesia, internal report.

Tri Handoko, B., 2009b: *Well completion test report LHD-34*. PT. Pertamina Geothermal Energy, Indonesia, internal report.

Tri Handoko, B., 2009c: *Well completion test report LHD-31*. PT. Pertamina Geothermal Energy, Indonesia, internal report.

Tri Handoko, B., 2010: *Well completion test report LHD-32*. PT. Pertamina Geothermal Energy, Indonesia, internal report.

Williams, C.F., 2007: Updated methods for estimating recovery factors for geothermal resources. *Proceedings of the 32nd Workshop on Geothermal Reservoir Engineering, Stanford University, Stanford*, 7 pp.

Witherspoon, P.A., Javandel, I., Neuman, S.P. and Freeze, R.A., 1967: *Interpretation of aquifer gas storage conditions from water pumping tests.* Amer. Gas Assoc., Monograph, 273 pp.

Yani, A., 2006: Numerical modelling of Lahendong geothermal system, Indonesia. *Report 24 in: Geothermal Training in Iceland 2006*, UNU-GTP, Iceland, 547-580.

Zais, E.J., and Bodvarsson, G., 1980: *Analysis of production decline in geothermal reservoirs*. Geothermal Reservoir Engineering Management Program, Earth Science Division, Lawrence Berkeley Laboratory, University of California, Berkeley.